

Mars Global Digital Dune Database and initial science results

Rosalyn K. Hayward,¹ Kevin F. Mullins,² Lori K. Fenton,³ Trent M. Hare,¹
Timothy N. Titus,¹ Mary C. Bourke,^{4,5} Anthony Colaprete,⁶ and Philip R. Christensen⁷

Received 11 May 2007; revised 3 August 2007; accepted 4 September 2007; published 20 November 2007.

[1] A new Mars Global Digital Dune Database (MGD³) constructed using Thermal Emission Imaging System (THEMIS) infrared (IR) images provides a comprehensive and quantitative view of the geographic distribution of moderate- to large-size dune fields (area >1 km²) that will help researchers to understand global climatic and sedimentary processes that have shaped the surface of Mars. MGD³ extends from 65°N to 65°S latitude and includes ~550 dune fields, covering ~70,000 km², with an estimated total volume of ~3,600 km³. This area, when combined with polar dune estimates, suggests moderate- to large-size dune field coverage on Mars may total ~800,000 km², ~6 times less than the total areal estimate of ~5,000,000 km² for terrestrial dunes. Where availability and quality of THEMIS visible (VIS) or Mars Orbiter Camera narrow-angle (MOC NA) images allow, we classify dunes and include dune slipface measurements, which are derived from gross dune morphology and represent the prevailing wind direction at the last time of significant dune modification. For dunes located within craters, the azimuth from crater centroid to dune field centroid (referred to as dune centroid azimuth) is calculated and can provide an accurate method for tracking dune migration within smooth-floored craters. These indicators of wind direction are compared to output from a general circulation model (GCM). Dune centroid azimuth values generally correlate to regional wind patterns. Slipface orientations are less well correlated, suggesting that local topographic effects may play a larger role in dune orientation than regional winds.

Citation: Hayward, R. K., K. F. Mullins, L. K. Fenton, T. M. Hare, T. N. Titus, M. C. Bourke, A. Colaprete, and P. R. Christensen (2007), Mars Global Digital Dune Database and initial science results, *J. Geophys. Res.*, 112, E11007, doi:10.1029/2007JE002943.

1. Introduction

[2] Sand dunes are among the most widespread aeolian features present on Mars, serving as unique indicators of the interaction between the atmosphere and surface. In general subaerial dunes form where a source of sand-sized grains exists. These materials are carried downwind by winds of saltation strength, and they are ultimately deposited where winds weaken below the threshold for sand transport [Bagnold, 1941]. As a result, the study of dune processes contributes to both atmospheric and sedimentary science. Both the presence and morphology of sand dunes are sensitive to subtle shifts in wind circulation patterns and strengths, which are themselves influenced by changes in Martian orbital parameters [Haberle *et al.*, 2003]. The

spatial distribution of aeolian sand relates to patterns of sedimentary deposition and erosion of source materials, giving clues to the sedimentary history of the surrounding terrain [e.g., Edgett, 2002; Byrne and Murray, 2002; Fenton, 2005]. Dunes are particularly suited to comprehensive planetary studies because they are abundant on the Martian surface over a wide range of elevations and terrain types. Thus a global-scale study of Martian dunes serves a dual purpose in furthering our understanding of both climatic and sedimentary processes, two fundamental topics currently driving Martian science.

[3] Previous aeolian studies of the Martian surface relied on Mariner 9 and Viking Orbiter images to examine and map aeolian morphologies [McCauley *et al.*, 1972; Cutts and Smith, 1973; Ward *et al.*, 1985]. More recent studies, using high-resolution images like Mars Global Surveyor (MGS) Mars Orbiter Camera narrow-angle (MOC NA) [Malin *et al.*, 1992] and Mars 2001 Odyssey Orbiter Thermal Emission Imaging System (THEMIS) visible range images (VIS) [Christensen *et al.*, 2004], have enabled scientists to re-examine surficial areas from earlier investigations and see new aeolian deposits unresolved by previous instruments [e.g., Malin *et al.*, 1998; Edgett and Malin, 2000; Fenton *et al.*, 2002, 2003; Bourke *et al.*, 2004b]. As a result of the influx of high-resolution data, the Martian stratigraphic column is undergoing rapid evolution [Edgett, 2005] as are the interpretations of much of

¹Department of Astrogeology, U.S. Geological Survey, Flagstaff, Arizona, USA.

²Science Department, Coconino Community College, Flagstaff, Arizona, USA.

³Carl Sagan Center, NASA Ames Research Center, Moffett Field, California, USA.

⁴Planetary Science Institute, Tucson, Arizona, USA.

⁵University of Oxford, Oxford, UK.

⁶NASA Ames Research Center, Moffett Field, California, USA.

⁷Department of Geological Sciences, School of Earth and Space Exploration, Arizona State University, Tempe, Arizona, USA.

Mars' geologic history [e.g., *Tanaka et al.*, 2003, 2005], contributing to new insights about Martian aeolian processes and relationships. Surface images from both orbiting spacecraft (e.g., from MGS MOC NA) and Mars Exploration Rovers (MER) demonstrate that erosional and depositional features of aeolian origin are ubiquitous on the Martian surface [*Malin et al.*, 1998; *Greeley et al.*, 2004]. While these studies are of scientific importance, none provides a comprehensive global catalog of Martian aeolian features at scales made possible by existing data sets.

[4] Current releases of THEMIS infrared (IR) images (100 m/px resolution) provide nearly complete coverage of the Martian surface. As such, these images can robustly serve as a basis for a planetwide inventory of moderate to large-scale dune deposits. Within a global context, dune forms and regional distributions can easily be compared to global data sets (e.g., Mars Orbiter Laser Altimeter (MOLA) elevations and Thermal Emission Spectrometer (TES) derived thermal inertia values) and models (e.g., General Circulation Models (GCMs)), to provide a better understanding of the planetwide processes that have shaped the Martian surface. We present here our initial science results based on MGD³, selecting the parameters of dune morphology, dune area, dune volume, slipface orientation, and crater centroid to dune field centroid azimuth (value is given GIS field name CcDcAz and is referred to hereafter as dune centroid azimuth), to illustrate how the information can be presented and analyzed using the database. Because we want to focus on the global nature of the database, the scope of study for this paper is broad. We do not attempt, for example, to look at slipface detail, but base our measurements on gross dune morphology, then compare the measurements to the GCM across the entire 65°N to 65°S region. The database could be used as well, however, to identify areas of interest for more detailed studies. Following a brief description of MGD³ we (1) present examples of dune morphology found throughout the 65°N to 65°S region and consider the implications for dune classification on Mars; (2) discuss areal and volumetric geographic distribution of dune fields, compare Martian and terrestrial size distributions and discuss possible reasons for observed differences; (3) show examples of our dune orientation measurement technique; (4) present examples of dune centroid azimuth values and their relationship to crater floor morphology; and (5) compare dune orientation and dune centroid azimuth values to GCM output, in a variety of environments and discuss the use of dune centroid azimuth values as a proxy for regional winds and a tool in tracing sand sources.

2. Method

[5] The methods employed to create MGD³ and all its derived attributes are described in detail in the auxiliary material¹ (see Text S1). Here we will give a brief description of its geographic extent, most important attributes and availability. Particular attention is given to how dune field polygons were identified for inclusion in the database. Our method limited the size of dune fields that could be detected

to moderate- and large-size dune fields, which should be remembered when interpreting our observations. While the moderate to large dune fields are likely to constitute the largest compilation of sediment on the planet, smaller stores of sediment of dunes are likely to be found elsewhere via higher-resolution data. The absence of mapped dune fields does not mean that such dune fields do not exist and is not intended to imply a lack of saltating sand in other areas. We also discuss the grid spacing and threshold value chosen for the GCM, as these are critical in interpreting dune orientation-GCM and dune centroid azimuth-GCM correlations.

2.1. Database Description and Availability

[6] MGD³, which extends from 65°N to 65°S latitude, provides researchers with a global geographic context for dune features, making it possible to examine the spatial distribution of aeolian features in a Geographic Information System (GIS) format. The area north of 65°N, where the majority of dunes are concentrated in the vast polar erg, and the area south of 65°S will be included in a later version of the database. The dune field vector file (as ESRITM shapefile) is the core of the dune database, along with eight other shapefiles that were created and used to derive much of the information supplied in the dune field attribute table (see auxiliary material Tables S1 and S2). For each of the ~550 dune fields in the database, the following attributes are among those provided: dune type based on higher-resolution imaging (THEMIS VIS and MOC NA); lists of images used to compile the database; areal extent; two volume estimates; MOLA-based average elevation; and dune orientation measured using THEMIS VIS and MOC NA images, where possible. In addition, crater diameter, crater area, and dune centroid azimuth are included when a dune field occurs within a crater or other circular depression (e.g., Nili Patera is included). For simplicity, the term crater includes all circular depressions. Output from the Ames Mars GCM [*Haberle et al.*, 1999], with attributes including shear stress, wind velocity and direction, is provided so that the attributes detailed above can be studied in the light of modeled atmospheric behavior. The height of the reported wind velocity varies with pressure and is typically between 3 and 8 meters above the surface.

[7] The full version of MGD³, with context and background files, including MOLA, MOLA-derived hillshades, and a geological map based on *USGS I-1802* [*Scott and Tanaka*, 1986] 1:15M scale, as digitized and reinterpreted by *Skinner et al.* [2006] is available on the Internet at <http://pubs.usgs.gov/of/2007/1158/> as a USGS Open File Report, OFR 2007-1158 [*Hayward et al.*, 2007]. The ~1800 MOC NA, THEMIS VIS and THEMIS IR images, used to construct the database, were processed and projected into GIS projects that are included in the USGS Open File Report. For more information on the contents, visit the Open File Report website. Selected database shapefiles are also available as layers on Arizona State University's JMARS website (<http://jmars.asu.edu>) and on the USGS Planetary GIS Web Server - PIGWAD (<http://webgis.wr.usgs.gov>). For non-GIS users, a full version (37 columns) of the dune field attribute table is provided (see auxiliary material Table S2). Due to the extensive volume of GCM output, it cannot be included in the tabular version of the database. For detailed descriptions of the files provided in

¹Auxiliary material data sets are available at <ftp://ftp.agu.org/apend/j/e/2007je002943>. Other auxiliary material files are in the HTML.

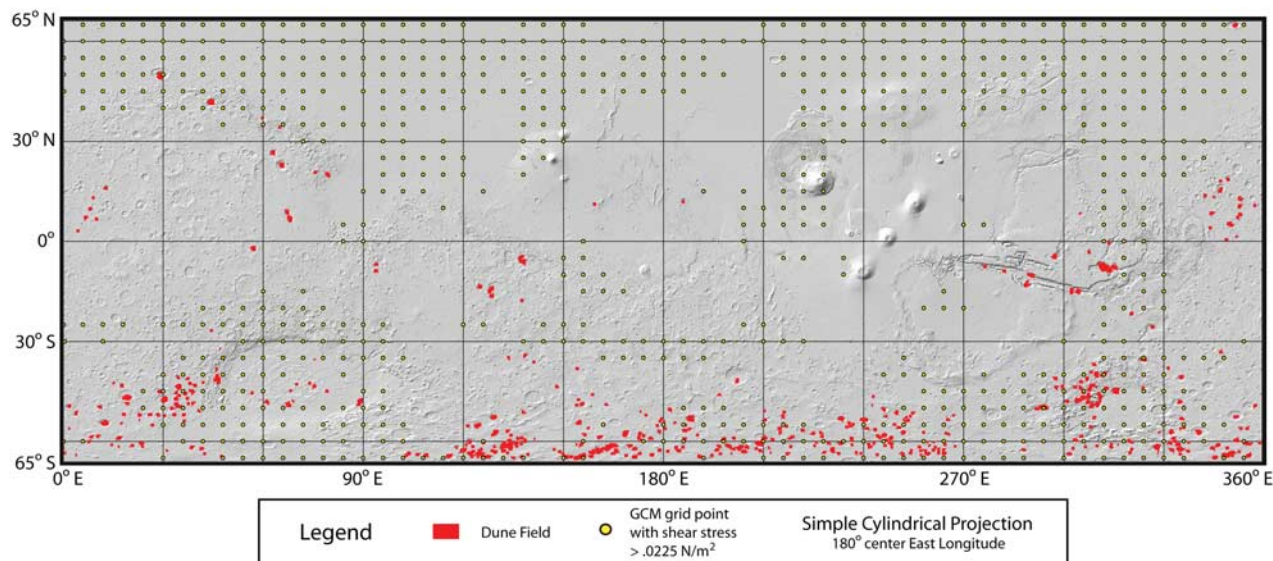


Figure 1. Geographic distribution of dune fields and GCM grid points between 65°N and 65°S latitude. Only GCM grid points with a shear stress value $>0.0225 \text{ N/m}^2$ are shown. Background is a MOLA-derived shaded relief map. Dune fields between 65°S and 90°S latitude and dune fields between 65°N and 90°N latitude are not included in Version 1.0 of the database.

the auxiliary material, refer to the “ReadMe” file. This paper will only discuss in detail those parameters selected for study here. Please refer to the USGS OFR 2007-1158 or auxiliary material for detailed descriptions of all parameters.

2.2. Creating Dune Polygons

[8] The database is based on dune forms and/or deposits that are located using calibrated THEMIS IR images (RDRs). An initial data set of THEMIS band 9 images covering orbits 816–9601 (spanning 02/2002–02/2004 and $L_s = 0.085^\circ - 358.531^\circ$), comprising more than 30,000 images planetwide, was chosen as the basis for the construction of the database. This provided 75% daytime and 98% nighttime coverage of Mars. Approximately 75% of the images identified as containing dunes were daytime images, where low-albedo dunes appear brighter than the surrounding area, indicating a warmer relative temperature. On nighttime images, where dunes are often darker than the surrounding area and show less tonal variation within a dune field, the dunes were more difficult to identify, so actual coverage may be closer to the 75% daytime coverage figure. Questionable dune fields were verified using higher-resolution THEMIS VIS or MOC NA images, where available. Because the initial location of dune fields is based on THEMIS IR images with a resolution of 100 m/px, only moderate to large-size dune fields are included in the database, with the smallest dune field covering an area of $\sim 1 \text{ km}^2$. We do not include bright, ripple-like bedforms. Figure 1 shows the geographic distribution of the MGD³ (~ 550 dune field polygons).

2.3. Dune Centroid Azimuths

[9] When a dune field was situated within a crater, we digitized the associated crater rim so that the crater’s spatial

relation to the dunes could be quantified. ESRI ArcMap[®] tools were used to locate the centroid (geographic center) of the crater, the centroid of the dune, and to calculate the azimuth between the centroids. We refer to the resulting geodesic azimuth as the dune centroid azimuth. When a dune field occupied a well defined crater within a larger crater, the inner crater was chosen as the one exerting the most influence on depositional processes and the centroid of the inner crater was used to calculate the azimuth. In 14 of the 407 craters, where multiple dune fields occupy the crater floor, we calculated and reported a separate dune centroid azimuth for each dune field. We did not force a centroid to fall within its polygon, therefore for irregular dune field polygons the centroid may fall outside the polygon. For such irregularly shaped dune fields and for dune fields truncated by an image edge, the dune centroid may not accurately represent the entire dune field. It should be noted that in the case of irregular dune fields, truncated dune fields, and multiple dune fields within a crater, we report the centroids and azimuths as calculated, but caution that the azimuths may be misleading. Also note that the length of the dune centroid azimuth arrow merely indicates a direction and does not imply wind velocity.

2.4. Modeled Wind Direction

[10] Grid spacing for the Ames Mars GCM is based on 5 degrees of latitude by 6 degrees of longitude cells. Output was created for each degree of solar longitude (L_s) in one Martian year. L_s measures the position of Mars relative to the sun in 360 degrees beginning at vernal equinox. Shear stress, wind velocity and wind azimuth were provided 8 times daily for each L_s , resulting in ~ 3000 vectors per grid location. Shear stress is the force imparted per unit area on the ground by the wind. Below a certain threshold shear

Table 1. Dune Classification Used in the Database

Dune Type	Abbreviation	Number of Type Assigned	Description
Sand sheet	SS	128	sheetlike with broad, flat surface, no slipfaces [McKee, 1979]
Dome	D	8	circular or elliptical mound, no slipfaces [McKee, 1979]
Barchan	B	144	crescent in plan view, 1 slipface [McKee, 1979]
Barchanoid	Bd	261	row of connected crescents in plan view, 1 slipface [McKee, 1979]
Transverse	T	91	asymmetrical ridge, 1 slipface [McKee, 1979]
Linear	L	27	symmetrical ridge, 2 slipfaces [McKee, 1979]
Star	S	6	central peak with 3 or more arms, 3 or more slipfaces [McKee, 1979]
Unclassified	U	275	dunes that could not be classified, usually due to a lack of suitably detailed images

stress, the wind does not exert enough force to move sand grains. Above this value, loose sand grains may move by saltation along the ground; this value is termed the threshold stress for sand saltation. *Haberle et al.* [2003] have shown that setting a threshold stress of 0.0225 N/m^2 with the Ames Mars GCM will lift dust (through bombardment from sand saltation) in spatial patterns that qualitatively agree with observed dust storm occurrences. While we have chosen the same threshold stress value in this work, it is possible that sustained movement of sand may require long-term winds significantly above this threshold. Figure 1 plots locations where the GCM predicted wind shear stresses are greater than 0.0225 N/m^2 . For more details about the Ames Mars GCM, see *Haberle et al.* [1999].

[11] The coarse grid spacing of the Ames GCM can provide a fairly accurate estimate of the wind azimuth. *Fenton and Richardson* [2001] found that even changing orbital parameters such as obliquity, eccentricity, and perihelion states did not change predicted surface wind orientations. However, the coarse grid spacing has the effect of smoothing wind velocities and wind shear stress output, so that extreme values are lost. Thus some grid points with winds capable of moving sand are left empty after application of the threshold. High-resolution modeling of the interaction between rough topography and wind patterns [*Bourke et al.*, 2004b] suggests that the presence of topographic barriers may create winds of increased velocity that are capable of entrainment. Only a much higher resolution grid cell than we are currently using can both retain extreme values and provide detailed model output reflecting local topography. Unfortunately, computer processing time and

the volume of output associated with such a model on a global scale make the exercise impractical at this time.

3. Applications of MGD³

[12] MGD³ serves as a context for global- and regional-scale studies relating to climate, sedimentology, and aeolian processes. On a global scale, we examine dune morphology, the geographic and size distributions of dune fields, slipface-GCM correlation and dune centroid azimuth-GCM correlation. On a regional scale, we examine how slipface-GCM correlations and dune centroid azimuth-GCM correlations vary with local environmental conditions.

3.1. Dune Morphology and Implications for Classification

[13] Experience has shown that classification based on THEMIS IR images alone is not reliable because image resolution is often not sufficient to reveal pertinent detail. Where available, THEMIS VIS and/or MOC NA images were used to confirm, modify or refine original polygon boundaries and to classify dune morphology.

[14] The images were located using the JMARS utility (<http://jmars.asu.edu/>) [*Gorelick et al.*, 2003], and radiometrically and geometrically processed using ISIS software [*Torson and Becker*, 1997; *Gaddis et al.*, 1997].

[15] We are using the classification of *McKee* [1979] as the basis for identifying dune forms. Previous studies that were based on Viking 1 and 2 Orbiter images also classified dunes on the basis of knowledge of terrestrial dunes. Dune forms previously identified on Mars include barchan, barchanoid, transverse, dome, or complex (dunes that combine

Figure 2. Examples of dune types used to classify dune fields, based on *McKee's* [1979] Earth-based classification system. Each image description includes dune type, image ID number, dune field ID number, longitude and latitude of dune field centroid, and discussion, if needed: (a) barchan, E0902707, 0304-475, 30.4°E, 47.5°S; (b) barchan, R0300926, 1370-050, 137.0°E, 5.0°S; (c) barchan, M0204432, 0194-468, 19.4°E, 46.8°S, some joining of dunes; (d) barchan, R0400598, 1283-141, 128.3°E, 14.1°S, elongated horns on one side indicate influence of secondary wind direction; (e) barchanoid, M2300263, 1283-141, 128.3°E, 14.1°S, dune field occurs within large (~300 km diameter) crater; detail here shows barchanoid dunes nearly obscuring small (~1 km diameter) crater; (f) barchanoid, E0302016, 0671 + 088, 67.1°E, 8.8°N, edge of dune field in Nili Patera, shows transition from barchans with elongated horns to barchanoid; (g) barchanoid, E0302016, 0671 + 088, 67.1°E, 8.8°N, same image and dune field as in Figure 2f, but shows interior of dune field where barchanoid form is more uniform; (h) barchanoid, V01048003, 0347-437, 34.7°E, 43.7°S; (i) transverse, M0806802, 2938-497, 293.8°E, 49.7°S; (j) transverse, R1001964, 1586-633; 158.6°E, 63.3°S; (k) barchan, barchanoid and transverse, M0806802, 2938-497, 293.8°E, 49.7°S, dune types shown as they occur together in a dune field; (l) dome, R1901441, 0380-447, 38.0°E, 44.7°S; (m) linear, M2001808, 0168-589, 16.8°E, 58.9°S; (n) linear, S0201094, 1376-059, 137.6°E, 5.9°S; (o) star, R0300863, 2975-411, 297.5°E, 41.1°S; (p) star, M0702777, 0304-475, 30.4°E, 47.5°S; (q) sand sheet, E1302032, 2086-603, 208.6°E, 60.3°S; (r) sand sheet, V08533005, 1713-646, 171.3°E, 64.6°S; (s) sand sheet, V09981003, 1612-626, 161.2°E, 62.6°S.

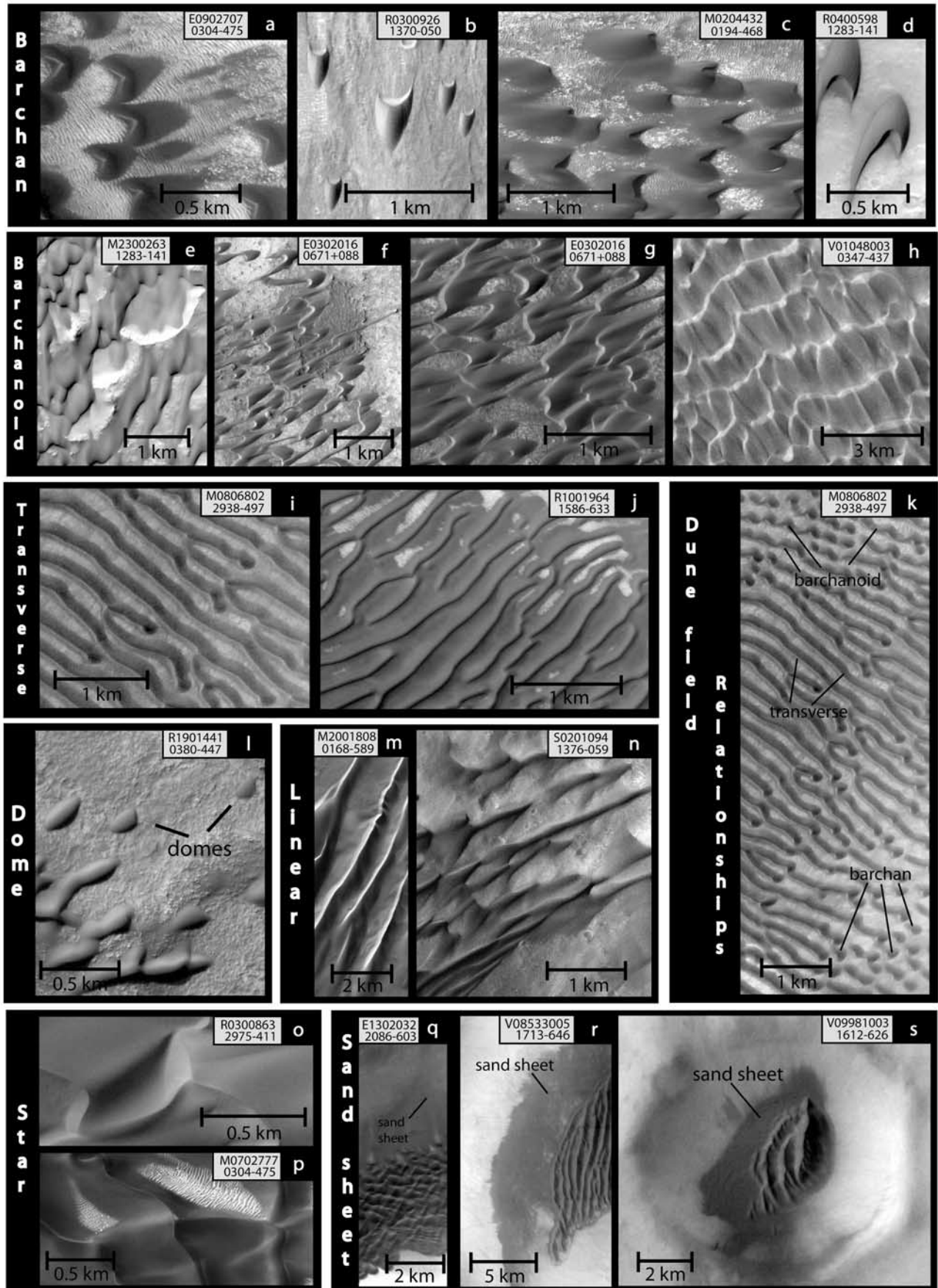


Figure 2

aspects of other types) [Cutts and Smith, 1973; Breed, 1977; Breed et al., 1979; Tsoar et al., 1979; Cwick and Campos-Marquetti, 1983; Thomas, 1984; Ward et al., 1985]. Isolated examples of star and linear dunes have also been found [Edgett and Christensen, 1994; Lee and Thomas, 1995]. In addition, recent studies noted the presence of compound dunes (not previously reported on Mars) as well as several varieties of transverse ridges [Bourke et al., 2003, 2004a; Balme and Bourke, 2005].

[16] Our classification includes McKee's sheet (our sand sheet), dome, barchan, barchanoid, transverse, linear and star dune types (Table 1 and Figure 2). Barchan, barchanoid and transverse dunes form under similar conditions, frequently occur together and grade into each other (Figure 2k). They are sometimes grouped together and referred to as crescentic or barchanoid dunes [McKee, 1979]. Here we use them as separate dune types. The classifications and abbreviations of dune types are listed in Table 1; Figure 2 shows examples of the dune types. Applying terrestrial classifications to Mars dunes, which have formed under somewhat different environmental conditions, can be a complex task. We attempt to fit dune forms into the terrestrial classification they most resemble; however, when transitional forms are found that do not fit, we label them as "unclassified." For example, McKee defines barchans as crescent in plan view with one slipface, indicating one predominant direction of wind (Table 1). The first three images of barchans, Figures 2a–2c fit McKee's description, although the barchans in Figure 2c are beginning to join together. The dunes in Figure 2d have been modified by a secondary wind direction, causing elongation of one of the barchan horns, a response seen in terrestrial dunes. In Figure 3a, the modification is more unusual, resulting in two slipfaces. These and similar dunes have also been referred to as "tear drop," "wedge," or "bifacial" dunes by De Hon [2006]. They do not fit into McKee's classification and so are "unclassified."

[17] Figures 2e–2h illustrate the range in barchanoid dune forms, with Figure 2e exemplifying typical barchanoid dunes, defined by McKee as a row of connected crescents in plan view, with 1 slipface. Figure 2f shows barchanoid dunes at the edge of the dune field where individual barchan shapes can still be distinguished, but the dunes have started

to merge and connect. Merging is more complete and uniform in Figure 2g, where the individual barchan shapes are nearly lost. In Figure 2h all sense of individual barchans, including bare interdune area, is gone. Barchanoid dunes sometimes grade into transverse dunes (Figures 2i and 2j), defined as asymmetrical ridges with one slipface. Figure 2k illustrates a typical relationship among dune types within a dune field, with barchans near the edge of a dune field, grading inward to barchanoid and then transverse dunes. Domes, circular or elliptical mounds of sand with no slipfaces, are shown in Figure 2l. Linear dunes (Figures 2m and 2n) are defined as symmetrical ridges with 2 slipfaces and star dunes, as central peaks with 3 or more arms and 3 or more slipfaces (Figures 2o and 2p). Sand sheets, broad expanses of sand with a flat surface and no slipfaces (Figures 2q–2s), can occur alone or adjacent to other dune forms. Figures 3a–3f show dune forms labeled "unclassified" because it is unclear where to place them in McKee's system. Figures 3b, 3c and 3e may be barchan and barchanoid dunes, modified by local topography. Figure 3d could be showing compound dunes, with smaller transverse dunes covering larger transverse dunes. However, it is also possible that the smaller secondary features could be erosional and thus for now remain "unclassified." Figure 3f shows a dune form, unusual by terrestrial standards, that is sometimes found in Martian craters. These "unclassified" dunes, labeled "unusual morphology" in Figures 3a–3f, might argue for some modifications to the terrestrial-based classification system when applied to Martian dunes. Dunes were also designated as "unclassified" if they were identified solely on the basis of THEMIS IR images, or if they could not be classified with available THEMIS VIS or MOC NA images due to inadequate image quality (Figures 3g–3l).

3.2. Areal and Volumetric Distributions of Mars Dune Fields and Comparison to Terrestrial Distribution

3.2.1. Dune Field Area

[18] The area of a given dune field is calculated in the sinusoidal projection based on the extent of the digitized dune field polygon. However, exact dune field boundaries can be difficult to identify, and therefore dune field area can be difficult to quantify. For example, some polygons cover

Figure 3. Examples of dune types used to classify dune fields; these examples are from "unclassified" dune fields. Each image description includes dune type, image ID number, dune field ID number, longitude and latitude of dune field centroid, and discussion, if needed: (a) unclassified, E2100192, 3347-481, 334.7°E, 48.1°S, dune morphology does not exactly fit that seen in Earth barchans; may be modified barchan influenced by 2 wind directions; also referred to as "incipient barchan" and "fortune cookie" dunes [De Hon, 2006]; (b) unclassified, E0502302, 3499 + 053, 349.9°E, 5.3°N, multidirectional winds and local topography may modify these dune forms; small dunes on northwest edge may be similar to De Hon's [2006] wedge dunes; (c) unclassified, M0400732, 0656 + 228, 65.6°E, 22.8°N, may be barchanoid modified by multidirectional wind and local topography; (d) unclassified, E1302032, 2086-603, 208.6°E, 60.3°S, may be complex or compound, with transverse superimposed on barchanoid or transverse; (e) unclassified, E1103140, 2763-076, 276.3°E, 7.6°S, local topography probably influences winds; better resolution image may allow classification; (f) unclassified, V09982002, 1327-611, 132.7°E, 61.1°S; (g) unclassified, V17849011, 3573-492, 357.3°E, 49.2°S, may be linear and dome; (h) unclassified, V14425004, 1250-639, 125.0°E, 63.9°S, frost on dunes prevents classification; (i) unclassified, I07486004, 1250-639, 125.0°E, 63.9°S, same dune as in Figure 3h, bright tone of THEMIS IR and form indicates dunes, but detail insufficient for classification; (j) unclassified, I08448002, 0887-488, 88.7°E, 48.8°S, bright tone of THEMIS IR and form indicates dunes, but detail insufficient for classification; (k) unclassified, I07738004, 0611-481, 61.1°E, 48.1°S, bright tone of THEMIS IR and form indicates dunes, but detail insufficient for classification; (l) unclassified, I07486004, 1247-632, 124.7°E, 63.2°S, bright tone of THEMIS IR and form indicates dunes, may be transverse and sand sheet, but detail insufficient for classification.

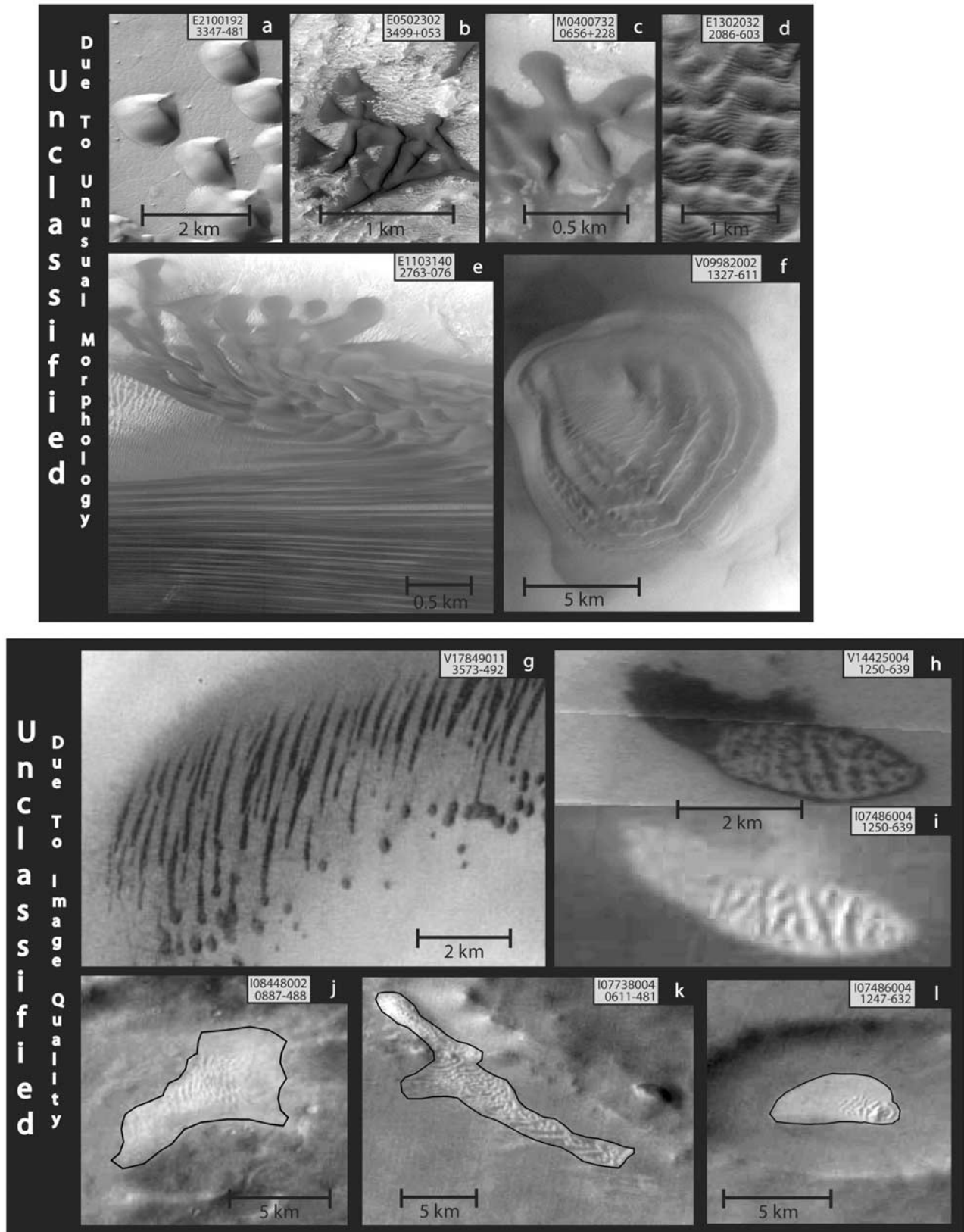


Figure 3

Table 2. Summary of Distribution of Dune Field Polygons in Narrow, 10° Latitude Bands and in 4 Broader Bands

Latitude Range, degrees	Number of Dune Fields	% of Total Number of Dune Fields	Area, km ²	% of Total Area	Volume 1, km ³	Volume 2, km ³
<i>Narrow Bands</i>						
−65/−55	284	51.9	25,924.95	37.17	3461.44	1286.34
−55/−45	117	21.4	17,981.31	25.78	3777.03	966.53
−45/−35	59	10.8	5821.04	8.35	2330.28	314.41
−35/−25	7	1.3	315.6	0.45	29.17	15.88
−25/−15	8	1.5	1021.77	1.46	269.92	56.75
−5/−15	23	4.2	10,473.15	15.02	3529.44	542.57
+5/−5	9	1.6	1755.63	2.52	589.79	100.23
+5/+15	20	3.7	3001.03	4.30	477.77	153.75
+15/+25	10	1.8	1632.83	2.34	252.31	83.58
+25/+35	3	0.5	360.99	0.52	196.64	20.7
+35/+45	2	0.4	691.27	0.99	90.88	35.95
+45/+55	4	0.7	471.06	0.68	141.71	24.18
+55/+65	1	0.2	299.53	0.43	22.78	17.67
Totals	547	100	69,750.16	100	15,169.16	3618.54
<i>Broad Bands</i>						
−30/−65	465	85.0	49,803.32	71.4	9,572.85	2570.71
0/−30	37	6.8	13,274.69	19.0	4,372.36	701.35
0/+30	36	6.6	5165.39	7.4	966.66	266.65
+30/+65	9	1.6	1506.77	2.2	256.98	79.84

what appear to be thick, continuous dunes with clearly discernable boundaries at the edge of the dune field, while other dune fields grade into thinning sand sheets with indistinct boundaries. Still other dune field polygons encircle barchan swarms with barren interdune areas. Current areal estimates do not remove the barren interdune areas and thus overestimate dune area. Underestimates of dune area occur when dune fields are truncated at image boundaries.

3.2.2. Dune Field Volume

[19] The volume of a given dune field was estimated using two simple methods designed to arrive at a broad total estimate. For a detailed explanation of both, refer to auxiliary material Text S1. The first method was done within ESRI ArcMap[®] software using MOLA gridded topography to define the base and upper surface of the dune field polygons. ArcMap[®] typically chooses the lowest elevation within the polygon as the base of the dunes. Therefore, when dune fields occur in topographically complex environments, ArcMap[®] will tend to overestimate dune field volume. Initial total volume, estimated using Method 1, is $\sim 15,000$ km³. Choosing a more appropriate base elevation for five large dune fields where a small portion of the dune field extended into an adjacent topographic low, reduces the estimated total volume for Method 1 to $\sim 13,400$ km³. Since overestimation undoubtedly exists in other dune fields, this is an upper limit estimate of dune volume.

[20] Method 2 estimates volume by multiplying the area of the dune polygon by a Mean Dune Height (MDH). Method 2 mitigates the overestimation problem, caused by irregular topography, by calculating MDH using only those dune fields whose standard deviation (of elevation differences) falls at or below the median standard deviation of all dune field polygons. We attempt to further refine the estimation by taking into account the possible difference in thickness of different dune types [Wasson and Hyde, 1983]. This method results in an estimated total volume of

~ 3600 km³, substantially lower than the $\sim 13,400$ km³ found with Method 1. While ~ 3600 km³ provides a more realistic total volume, it may still be an overestimation. A detailed description of Method 1 and Method 2 is provided in the auxiliary material (see Text S1).

3.2.3. Areal Dune Field Distribution

[21] A global dune database for Mars has the potential to address local- to regional-scale aeolian processes by providing an important link between the geographic distribution of dune fields and their local, physical characteristics. Our database will also allow users to document global scale trends in aeolian activity. At a glance, Figure 1 shows that the majority of dune deposits in the database are located in the Martian southern hemisphere, scattered across the highlands terrain. Table 2 summarizes, by latitude, in 13 narrow bands and in 4 broader bands, the distribution of dune fields. The database contains ~ 550 dune polygons, covering $\sim 70,000$ km², between 65°N and 65°S latitude. 85% of the documented dune fields are situated between 30°S and 65°S latitude. They cover $\sim 50,000$ km², making up 71% by area of all dune fields in the database. A closer look at the southern hemisphere distribution shows a progressive increase in the number, area and volume of dunes, poleward from the equator. This poleward increase may have implications for the location of source material. Between 0° and 30°S latitude, 37 dune fields cover $\sim 13,000$ km². The corresponding band north of the equator (i.e., 0° to 30°N latitude) contains 36 dune fields, covering only ~ 5200 km². In the northernmost region covered by the database (i.e., 30° to 65°N) a scant 8 dune polygons were located, totaling $\sim 1,500$ km².

[22] Within the latitudinal trends, longitudinal trends can also be discerned. Of the 36 dune fields in the 0° to 30°N band, 33 dune fields are located between 340°E and 80°E (quadrangles MC-11 through MC-13). They contain $\sim 97\%$ of the ~ 5200 km² total area of dune fields within the 0° to 30°N band. Between 0° and 30°S latitude, 24 of the 37 dune

Table 3. Summary of Distribution of Dune Fields in Craters and Estimated Volumes for Selected Areas

Latitudinal Region	Number of Dune Fields	Volume of Dune Fields (Method 2), km ³	Number of Dune Fields in Craters	Volume of Dune Fields in Craters, km ³	% of Dune Fields in Craters (by Volume)
0° to 30°S	37	701	17	227	32
30° to 65°S	465	2571	368	2077	81
Argyre Planitia and surrounding rough terrain	47	265	12	127	48
Hellas Planitia and surrounding rough terrain	18	72	2	5	7
Valles Marineris	20	474	0	0	0

fields, with a combined area of ~ 9500 km², are concentrated in and around Valles Marineris between 265°E and 315°E longitude.

[23] A trend that is clear across all geographic locations is that the majority of dune fields (78%, totaling nearly 50,000 km²), formed within craters. Between 0° and 65°S latitude, there are ~ 385 crater-related dune fields with a cumulative area of $\sim 44,000$ km², while between 0° to 65°N, there are ~ 40 crater-related dune fields with an area of ~ 5700 km².

3.2.4. Volumetric Dune Field Distribution

[24] The total dune field volumes reported here (Tables 2 and 3), range from a low of ~ 3600 km³ to a high of $\sim 15,000$ km³. Table 2 summarizes the distribution of these volumes according to latitude in four broad bands, 30° to 65°S, 0° to 30°S, 0° to 30°N, and 30° to 65°N. Using Method 2, we estimate that ~ 2570 km³ of dunes are concentrated between 30° and 65°S, ~ 700 km³ between 0° and 30°S, ~ 270 km³ between 0° and 30°N, and ~ 80 km³ between 30° and 65°N. Table 3 compares volumes of dune fields within craters to those outside craters for the 0° to 30°S and 30° to 65°S regions, as well as for the Hellas Planitia, Argyre Planitia, and Valles Marineris regions. For Hellas Planitia and Argyre Planitia, the area summarized includes the basins and the surrounding rough terrain. The Argyre Planitia and surrounding rough terrain contained 47 dune fields, including 12 in craters. The total volume of the dune fields is estimated to be ~ 265 km³ with ~ 130 km³, or $\sim 50\%$, residing in craters. The Hellas Planitia and surrounding rough terrain contained 18 dune fields, including 2 in craters (not counting Hellas Planitia as a crater itself). The total volume of the dune fields is estimated to be ~ 70 km³ with ~ 5 km³, or $\sim 7\%$, residing in craters. Valles Marineris contained 20 dune fields with a total volume of ~ 475 km³.

3.2.5. Dune Field Distribution: Comparison of Martian and Terrestrial Dune Fields

[25] *Wilson* [1973] compiled a comprehensive study of ~ 800 terrestrial dune fields, with some updates listed by *Cooke et al.* [1993] and *Livingstone and Warren* [1996] and references within. It is unclear what data *Wilson* [1973] used to compile his study (e.g., fieldwork versus spacecraft images), although he states that global estimates made for dune fields with areas smaller than 8000 km² are based on an extrapolation from Central Saharan dune fields, and are assumed to be representative of aeolian processes on the Earth. Therefore we note that the method used to compile terrestrial data is different from ours, resulting in areal

estimates that may not be accurate. Because the terrestrial study estimated dune field area rather than dune field volume, we compare terrestrial values to our Martian areal estimates rather than our volume estimates.

[26] The largest dune fields on Earth have areal extents in excess of 500,000 km², values that alone overshadow our Martian areal estimate for moderate- to large-size dune fields of $\sim 70,000$ km². Adding in the north polar sand seas, with a total estimated area of 680,000 km² [*Lancaster and Greeley*, 1990], and preliminary estimates of our database (not shown) poleward of 65°S of $\sim 50,000$ km², the total Martian dune field area of $\sim 800,000$ km² falls short of total terrestrial values of $\sim 5,000,000$ km². *Wilson* [1973] found that 85% of the areal coverage of sand occurs in dune fields larger than 32,000 km², suggesting that there is a “natural” size into which terrestrial dune fields grow. Because of this break in size, *Cooke et al.* [1993] define a “sand sea” as a dune field with an areal extent greater than 30,000 km². Similarly, we find that the 58 largest Martian dune fields (>300 km²) in our study area (i.e., not counting the north polar sand seas), account for 60% of the total areal coverage of dune sand. It should be noted that our estimate is for dark dunes. Including areal coverage for other bedforms such as transverse aeolian ridges (TARs) may significantly increase the total areal coverage of aeolian bedforms on Mars [*Balme and Bourke*, 2005]. For example, M. R. Balme (personal communication, 2007) has found that between 0° and 45°E longitude and 0° and 30°N latitude, the TARs (which may have no terrestrial counterpart) cover ~ 6 –7% of the surface.

[27] Figure 4 shows the distribution of Martian dune field sizes as a function of both number and area. Figure 4 may be compared to Figure 6 of *Wilson* [1973] (also Figure 28.1 of *Cooke et al.* [1993] and Figure 6.1 of *Livingstone and Warren* [1996]), although it should be noted that our abscissa ranges from 7.81–8000 km² compared to their 63–1,024,000 km² range. In Figure 4, the frequency of dune fields peaks at a size of ~ 30 km², dropping off at both larger and smaller values. The drop is steeper for larger dune field areas, with the slope rolling off at ~ 2000 km². In contrast, *Wilson* [1973] shows a steady and rapid drop from the smallest to the largest dune fields, with a change in slope at ~ 8000 km², a size four times that found for Mars. It is possible that there is also a drop with decreasing dune field area on Earth, but *Wilson*'s study may not have extended to a small enough areal extent. Regardless, the distributions indicate that there are many more large dune fields (and sand seas) on Earth than there are on Mars. This result

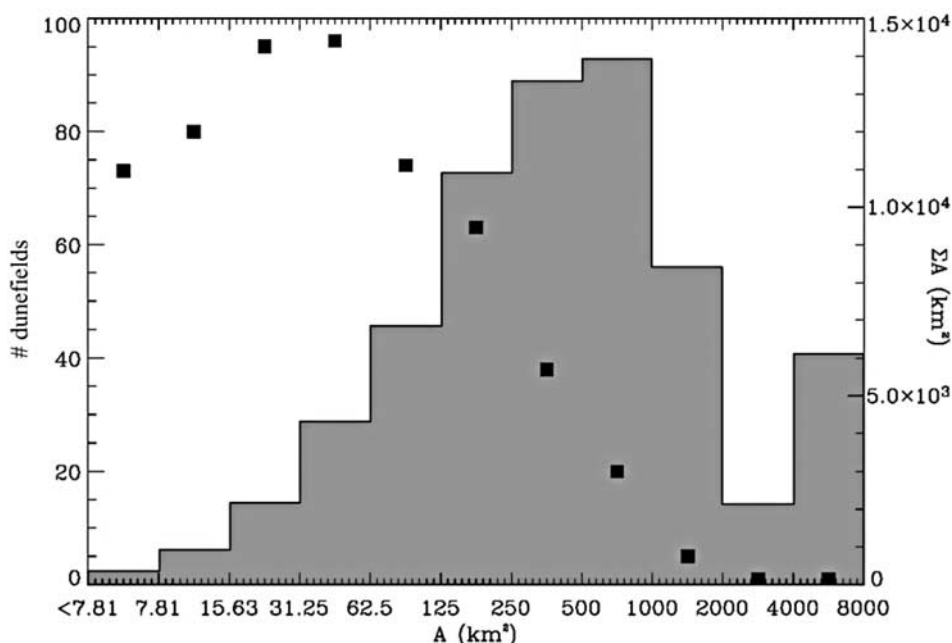


Figure 4. Frequency and area histograms of Martian dune fields in this study. Solid black boxes show the number of dune fields within a given areal bin size (frequency histogram, using the left vertical axis). The gray shaded region shows the total area covered by all of the dune fields within a given bin size (areal histogram, using the right vertical axis). There is a peak in dune field frequency at 30 km², suggesting that there is a characteristic dune field size on Mars. The areal histogram is bimodal with peaks at 500 km² and 4000 km², indicating that despite the abundance of dune fields smaller than 100 km², most of the dune sand is concentrated in dune fields larger than 100 km². Compared to the distribution of terrestrial dune field sizes, Martian dune fields are nearly as numerous but much smaller in areal extent. The smaller dune field sizes are likely caused by differences in basin size, sand supply rates, and wind energy between Earth and Mars.

contrasts with the previous perception in the planetary science community that the dark dunes on Mars are both larger and more extensive than dunes on Earth.

[28] The areal frequency of dune sand in Figure 4 is bimodal, with peaks at 500 km² and 4000 km². Although it is not discussed by *Wilson* [1973] or *Cooke et al.* [1993], there are peaks in terrestrial dune field sizes at 1000 km² and 4000 km², although these peaks are much more subtle than the jump at 32,000 km². It is unclear what causes these jumps in terrestrial dune field sizes and whether they could be similar to what we find on Mars. It is also unclear what implications, if any, these areal distribution peaks have for the formation, age, or growth of dune fields on Earth and Mars.

[29] The difference in dune field size distributions on Mars and Earth may be related to several factors. Terrestrial dune fields usually form in large, tectonically stable basins in regions with little rainfall and/or high evaporation rates. The sand accumulates downwind of a source region, generally where the net sand drift potential decreases because of converging winds or topographic changes [*Wilson*, 1973; *Cooke et al.*, 1993; *Livingstone and Warren*, 1996]. One possible difference between Mars and Earth is in the different topographic relief. Mars has numerous small topographic depressions on a scale of 300 km or less in locations where sand accumulates (e.g., craters), whereas

the largest terrestrial sand seas have formed in much larger basins. The largest of the Martian dune fields, the northern polar sand seas, are located on a vast low-lying plain like the deserts on Earth. It is possible that most of the sand supply on Mars is simply located in a different type of terrain (e.g., buried volcanic ash deposits, as opposed to alluvial deposits) than is typical of terrestrial deserts, keeping Mars from forming many large sand seas.

[30] Another possible difference between Mars and Earth may be the production rate of sand. The rate of production could be affected by both sand composition and weathering processes. Most dune sand on Earth is composed of quartz, whereas most dune sand on Mars is thought to be basaltic. On Earth, quartz weathers much more slowly than basalt. While the weathering rate of basalt under Mars-like conditions is unknown, it is possible that it may contribute to a difference in the rate of sand production between Mars and Earth. Weathering processes may also be different on Mars and Earth. Most terrestrial dune sand is produced by water-driven processes (i.e., along beaches, lakeshores, and rivers). The origin of Martian dune sand is unknown, but it is clear that in the present cold and dry environment, water is not capable of producing a great quantity of sand on Mars. It is possible that the relative abundance of terrestrial sand is related to the number and magnitude of water-related processes that provide a continual supply of sand.

[31] A final difference between the deserts on Mars and Earth is the wind regime. The thin Martian atmosphere must blow roughly an order of magnitude more strongly to lift sand into saltation relative to Earth [Greeley *et al.*, 1980]. All other factors being equal, the high saltation threshold will limit sand movement and lengthen timescales of bedform formation and reconstitution. It is possible that other landscape-changing processes on Mars bury or destroy dune fields at a fast rate relative to dune field formation, causing fewer dunes to be present at a given time than is observed on Earth. It is clear that there are many significant differences in the aeolian environment on Mars and Earth, each of which may contribute to differences in frequency and areal distributions.

3.3. Slipface Examples

[32] Dune slipface azimuth measurements were made using MOC NA and THEMIS VIS images. Although we refer to our measurements as slipface orientations or azimuths here and in the database, the downwind directions are actually identified through gross dune morphology (which often requires inspection of slipface positions). Thus our use of the term slipface does not imply the level of detail usually associated with the term. Slipface details are not always identifiable in VIS and MOC NA images, whereas gross dune morphology can be observed fairly clearly in images with different sun angles and resolutions, allowing for more complete and global determination of the wind directions that shape dunes.

[33] To further simplify our method, we only use the dunes that formed under unidirectional wind regime. It is generally accepted in terrestrial aeolian science that a multidirectional wind regime often creates nontrivial morphologies that require detailed study to decipher. For example, *Breed and Grow* [1979] show that the correlation between star dune diameters and their wavelengths (i.e., spacing) is much weaker than that for linear and crescentic dunes (i.e., barchan, barchanoid and transverse in our terminology). Such variations in morphology can make dunes that formed under multidirectional wind regimes difficult to identify and interpret. Our approach is to record the primary wind direction by averaging the individual slipface azimuths, discernable from gross dune morphology, of dune types formed by unidirectional winds (i.e., barchan, barchanoid and transverse). Fortunately, these three dune types were assigned to ~75% of the dune forms that we were able to classify (Table 1). The primary direction recorded is a proxy for the prevailing winds during the latest period of major dune modification. Any relatively minor changes to wind patterns or other atmospheric conditions that modify the dune slipface are considered secondary or tertiary and not recorded. We avoid using gross morphology of oblique dunes, thought to represent a combination of two acutely oriented winds, because only one wind would be identified as primary, and thus results would be misleading. Consequently, our method takes into account neither multidirectional winds that may be of nearly equal influence nor lesser secondary or tertiary winds, but concentrates on identifying prevailing wind direction, when it exists. Where there is evidence of multiple prevailing wind directions, that is, when some dunes in a field have gross morphologies that suggest different prevailing winds than

other dunes (and many large dune fields have perimeter barchans with opposing slipface orientations), we average and report them separately. Of the ~200 dune fields with slipface measurements, ~40 have two primary wind directions and ~15 have three primary wind directions.

[34] Figures 5a and 5b illustrate our method of slipface measurement on sharply defined barchan, barchanoid and transverse dunes. The vector begins on the upwind stoss slope and terminates on the lee slipface slope, indicating the direction of sediment transport and therefore the direction of prevailing winds during the latest period of major dune modification. In Figure 5c, adjacent THEMIS VIS (right side) and MOC NA (left side) images illustrate a case when gross dune morphology is clear enough in THEMIS VIS to draw slipface vectors. That decision is supported by the adjacent higher-resolution MOC NA image, where slipfaces are more sharply defined. In other cases, dunes may be too eroded or too frost covered (Figure 5d) to allow slipface measurement. In ~350 of the ~550 dune fields no slipfaces could be measured due to poor image resolution and/or quality, incomplete coverage, erosion, frost or other conditions. Note that arrow symbols are used only as directional indicators and are not meant to convey relative wind velocity. Slipface azimuths are not meant to be used as evidence for current dune activity, or to imply age constraints, as many of the identified dunes may be inactive.

3.4. Dune Centroid Azimuth Examples

[35] Dune field position within the crater and the relative area of a dune field, as a function of crater size and morphology, might be indicative of prevailing wind conditions at the time of dune formation or proximity to a source of sediment. Position and size of a dune field could also reflect the effects of crater topography (topographic traps within the crater or low crater rims). Dune centroid azimuth (section 2.3) was calculated for the approximately 78% of all dune fields in the database that are located within craters. This measurement is most meaningful where a single, regularly shaped, complete dune field occupies a single, smooth-floored crater (Figures 6a and 6b). In such cases, the centroid will accurately reflect the location of a dune field that was able to move unimpeded across the crater floor. In larger craters, where central peaks, younger impacts or erosion has created topographic traps or obstructions within the crater itself, the resulting crater floor roughness may influence the location of a dune field more than regional winds. This can result in multiple smaller dune fields with misleading azimuths (Figures 6c and 6d). Thus, under the right conditions (single dune field in smooth-floored crater), dune centroid azimuth can be used to quantify possible wind directions and long-term sediment transport as evidenced by dune field migrations, and therefore be of use as a first-order indication of regional prevailing wind patterns.

3.5. Comparison of Slipface and Dune Centroid Azimuth to GCM and Implications

[36] Much work has been done using the physical characteristics of aeolian bedforms to predict local and global wind patterns [e.g., *Ward*, 1979; *Greeley et al.*, 1993, 1999; *Fenton and Richardson*, 2001]. Though aeolian erosional and depositional processes are a function of climate, they

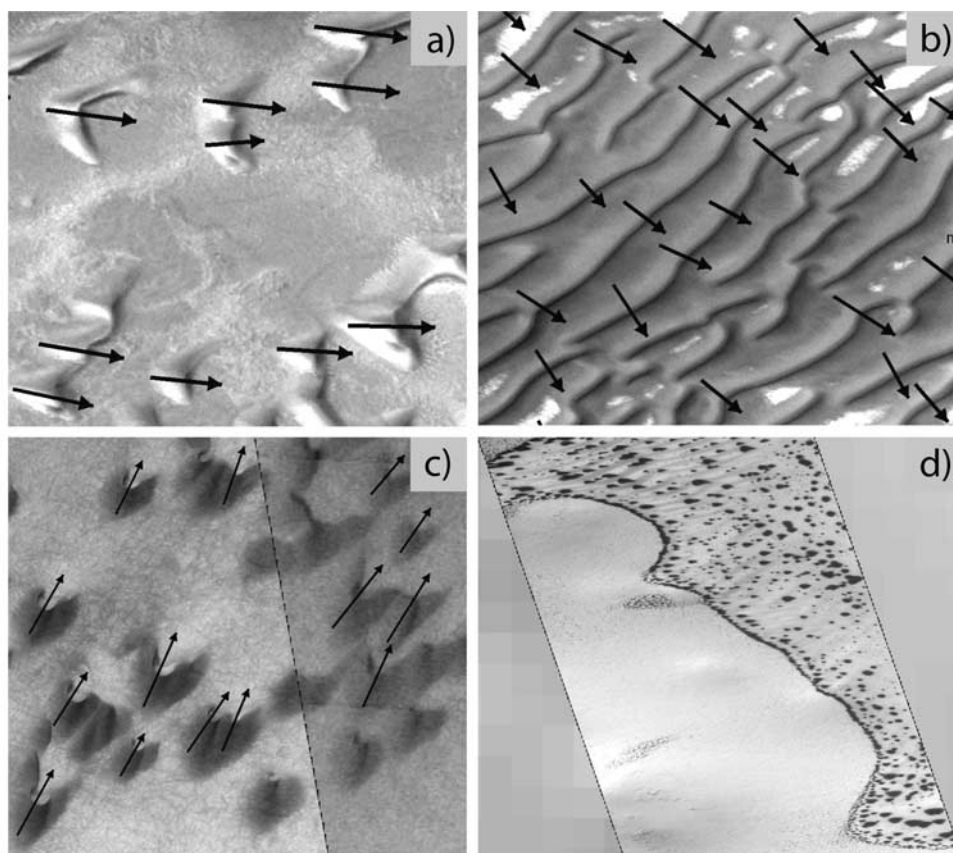


Figure 5. Images showing examples of representative dune forms and slipface vectors (or lack thereof). (a) MOC NA E0300630, dune ID 3347-481, showing slipface direction on classic barchan dunes; (b) MOC NA R1001964, dune ID 1586-633, showing slipface direction on barchanoid to transverse dunes; (c) VIS V07404005 overlain by MOC NA R1401899, dune ID 3352-407; note how the gross barchan morphology is quite clear on the lower-resolution VIS image; and (d) MOC NA M0402186, dune 3553-642, with unresolvable dune forms due to frost cover.

also provide a unique physical record of conditions at the boundary between the atmosphere and surface of a planet that can be used to interpret the environment under which they formed. The Martian aeolian record is important for several reasons: (1) it is extensive; (2) it is well exposed with distinct physical properties (e.g., thermal inertia, dune forms) that render it easily recognizable; and (3) it is well preserved, so that even inactive dunes yield information about the conditions under which they formed.

[37] Two physical characteristics of dune fields and dunes that can be measured as indications of primary wind directions are the geographic location of the dune field within the confines of a crater (dune centroid azimuth) and the slipfaces of the individual dunes within the dune field. These physical aspects cannot be measured for every dune field and even when they can, there is not always a valid GCM grid point ($>0.0225 \text{ N/m}^2$) available for comparison. While the threshold was carefully chosen, it should be noted that the coarse grid spacing of the Ames GCM has the effect of underestimating wind shear stress output. Therefore some winds capable of moving sand may not be available for comparison. Of the ~ 550 dunes in the database at this time, ~ 440 are within 360 km of a valid GCM grid point. Of those, ~ 340 dune fields are located within craters ($\sim 80\%$),

and thus will have a dune centroid azimuth measurement. Of the ~ 440 dune fields within 360 km of a valid GCM grid point, 135 have one or more primary slipface directions. Of the 135 dune fields with slipface measurements, 117 occur within a crater and also have dune centroid azimuth measurements, while 18 occur outside of craters and have only slipface measurements.

3.5.1. Dune Centroid Azimuth to GCM Comparison: Planetwide

[38] It is apparent from this global study of dune fields that dune centroid azimuth is a good indicator of regional winds (when crater floors are smooth), while slipface azimuth is more indicative of localized winds. Table 4 shows the breakdown of how well dune centroid azimuth correlates to the GCM based on crater diameter. For example, the table shows that there is an increase in correlation between dune centroid azimuth and GCM azimuths as crater diameter decreases, from $\sim 40\%$ agreement for the largest (craters $> 100 \text{ km}$) to $\sim 65\%$ agreement for the smallest (craters $< 25 \text{ km}$). Dune centroid azimuth appears to be influenced more by the relative smoothness of the crater floor than the actual crater diameter, but the smoothness of a crater floor is often a function of its size (i.e., no crustal rebound or overprinting by younger craters

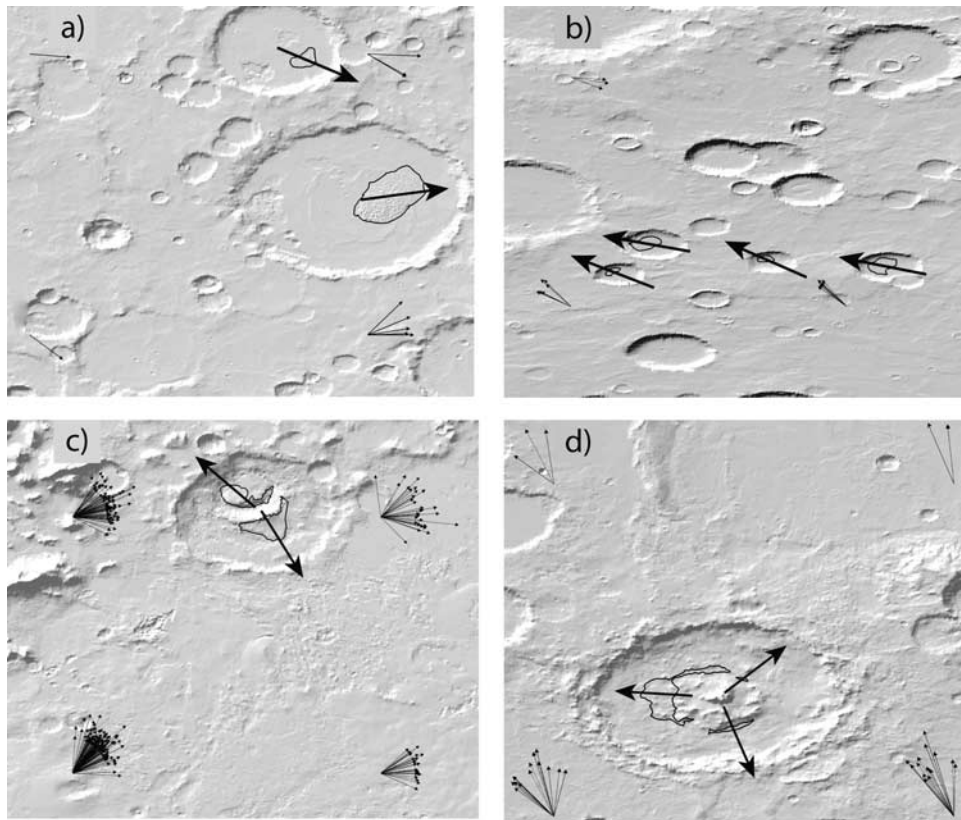


Figure 6. Four examples of dune fields in craters showing how the morphology of the craters can influence the location of deposition. Background of each is a MOLA-derived shaded relief map. Thin black arrows indicate the azimuths of wind shear stresses above 0.0225 N/m^2 [Haberle et al., 2003]; thick black arrows indicate the dune centroid azimuth. (a) Dune field 0304-475, in Proctor crater, a large (diameter $>100 \text{ km}$), smooth, flat-floored crater containing a large dune field that correlates well with the surrounding GCM azimuths. (b) From left to right, dune fields 1028-642, 1036-636, 1062-639, and 1087-641. Crater diameters range from 25 to 40 km, floors are smooth, and correlation between dune centroid azimuth and GCM is very good. (c) Dune fields 3153-446 and 3158-451, in a crater within a crater near the northern rim of the Argyre Planitia whose rough, chaotic floor prevents easy dune migration, resulting in no correlation between the dune centroid azimuth and the surrounding GCM azimuths. (d) Dune field 1877-531, a crater in the southern midlongitudes. The dune centroid azimuth of its largest field correlates well with the surrounding GCM wind predictions, but its minor associated dune fields are trapped by local topography, resulting in misleading dune centroid azimuth vectors.

causing topographic variations). If the crater is large enough to have a central peak or old enough to have more recent impacts upon its floor, then the topography of these features becomes a barrier in the migration path of the dunes. These topographic barriers can also affect local winds patterns and influence the distribution of the sand around the feature (Figures 6c and 6d). Figure 6a illustrates a case where, although the crater is large (diameter $> 100 \text{ km}$), the floor is smooth and the dune centroid azimuth correlates well with the GCM. If the craters are small ($<25 \text{ km}$) they are likely to have very smooth floors. Figure 6b shows small to moderate diameter (25 to 40 km) craters that have smooth floors with no topographic barriers or traps. The dunes were able to migrate unimpeded to their current location and so correlate well with the GCM.

[39] The direction of dune centroid azimuth gives a clue to sediment source. Some of the larger craters may contain source materials for their dune fields, in the form of nearby

pits or deep excavations, but the appearance of dune fields within smaller craters poses the question of their source. Smaller craters penetrate the substrate less and have no pits or deep excavations to provide source material [Fenton, 2005]. A more detailed look at dune centroid azimuth may help establish sediment transport pathways in the southern hemisphere.

3.5.2. Slipface to GCM Comparison: Planetwide

[40] When comparing Slipface (SF) to GCM, the influence of crater diameter is perhaps the opposite of that found when comparing dune centroid azimuth to GCM. The SF to GCM correlations are poor for intracrater dunes in all but the largest craters. As crater size decreases, the high relief of nearby crater walls would more strongly affect local winds over any interior dune fields, exerting an increasing influence on dune morphology. Rafkin et al. [2001] simulated wind flow around small (1 km diameter) craters, using the Mars regional atmospheric modeling system. While their

Table 4. Summary of Correlation of GCM to Dune Centroid Azimuth and Slipface Azimuth^a

	Number of Dune Fields Within 360 km	CcDcAz-GCM Correlation (Within $\sim 45^\circ$)	Percent CcDcAz-GCM Correlation (Within $\sim 45^\circ$)	Dune Fields With Slipface (SF)	Slipface-GCM Correlation (Within $\sim 45^\circ$)	Percent Slipface-GCM Correlation (Within $\sim 45^\circ$)
Diam > 100	30	12	40.0	22	13	59.1
Diam > 50 < 100	66	35	53.0	28	11	39.3
Diam > 25 < 50	136	74	54.4	43	11	25.6
Diam < 25	110	71	64.6	24	14	58.3
Total for intracrater dunes	342	192	56.1	117	49	41.9
Intercrater dunes	96	N/A	N/A	18	9	50.0
Total for all dunes	438	N/A	N/A	135	58	43.0

^aCcDcAz, dune centroid azimuth; SF, Slipface. Correlation means that GCM azimuth was within $\sim 45^\circ$ in either direction of the parameter being compared (either CcDcAz or SF azimuth). Only dune fields within 360 km of a GCM output $> 0.0225 \text{ N/m}^2$ are used. Four hundred thirty-eight dune fields were within 360 km of GCM; 342 of those were in craters.

work did not address the affect of crater size on flow within a crater, they did find that the presence of crater rims results in more complex atmosphere-surface interactions. We suggest that as the diameter of the crater increases, the distance from dune field to crater rim increases and the localized effects would decrease. This diminishing influence of the crater rim might explain the similar correlations of intercrater and large crater dune slipfaces (43% and 47%, respectively). Thus the dune morphology measurements appear to reflect regional wind patterns best on the intercrater plains and in very larger craters, whereas dune centroid azimuth measurements (see section 3.5.1) appear to reflect regional wind patterns best in smaller and/or smooth-floored craters.

3.5.3. Dune Centroid Azimuth to GCM Comparison: The Southern Midlatitudes

[41] Of the $\sim 10,000$ GCM shear stress values occurring above the grain movement threshold and located between 45°S – 65°S , $\sim 80\%$ of them fall between $\geq 280^\circ$ and $\leq 45^\circ$ azimuth, indicating that strong prevailing winds in the southern midlatitudes blow in a range from the ESE to SW. The largest modeled shear stress values ($> 0.04 \text{ N/m}^2$) occur from late southern winter through spring ($\sim L_s 128$ – 225) and autumn ($\sim L_s 10$ – 45). In the southern midlatitudes, $\sim 70\%$ of the dune centroid azimuth measurements correlate to GCM wind stress directions, a value considerably higher than the $\sim 55\%$ overall correlation for the entire 65°N to 65°S study area. When we break down GCM and dune centroid azimuth correlation by crater diameter we see a low of $\sim 58\%$ correlation for dune fields in craters with diameters $> 50 \text{ km}$ and a high of $\sim 76\%$ correlation for those in craters $< 25 \text{ km}$, suggesting that the above hypothesis regarding crater floor smoothness is applicable in this region (see section 3.5.2). Dune morphology orientations for the same area show only a $\sim 27\%$ correlation with GCM wind directions, increasing to only $\sim 30\%$ for dune fields within craters. Because we are correlating to the regional wind as predicted by a coarse GCM, when a dune field has more than one primary direction recorded, we use the direction that is based on the largest number of measurements.

[42] The high correlation of dune centroid azimuth measurements and the low correlation of dune morphology measurements with GCM wind stress directions may be caused by a number of factors. The disparity may relate to the distribution of crater sizes bearing dune fields, or in the complexity of the wind regime. Further study is required to understand what causes these differences, and why the

differences vary from region to region. Two regions in the southern midlatitudes illustrate how these measurements relate to the wind regime on Mars: south of Argyre Planitia and west of Hellas Planitia.

[43] South of Argyre Planitia, both GCM wind stresses and dune centroid azimuth measurements indicate that strong winds blow with a southerly component, as shown in Figure 7a. Unfortunately, no clear dune morphology measurements are available in this region to augment the dune centroid azimuth measurements. Off-cap winds are interpreted to spill into the local topographic low of Argyre, creating strong down-slope winds [Bass and Siili, 1999]. These early to late spring and summer winds may be manifested in the apparent migration of the dunes into the northern quadrants of craters south of Argyre, resulting in a good positive correlation between the dune centroid azimuth and GCM vectors.

[44] Our measurements for the western part of Hellas Planitia and eastern edge of Noachis Terra indicate a spatial shift in the correspondence between the dune centroid azimuth and the predicted GCM winds (see Figure 7b). The dune centroid azimuth measurements for dune fields over the highlands terrain correspond well to GCM predictions, as shown by the preponderance of blue vectors, used to represent dune centroid azimuths that agree with GCM output. Closer to the rim of Hellas an unpredicted wind with an easterly component apparently dominates. This area is defined by a concentration of red vectors, used to represent dune centroid azimuths that oppose the GCM predicted wind directions. Figure 7c shows that the dune morphology azimuths indicate a more multidirectional wind regime over both the highland terrain and the area adjacent to Hellas. In both areas sand-saltating winds that generally oppose the GCM (easterly winds, represented in red) and those that generally agree with the GCM (westerly winds, represented in blue) are more widely spread than the dune centroid azimuth measurements suggest. Fenton *et al.* [2005] use a mesoscale model to show that some of the winds, with easterly components, are represented by spring and summer evening katabatic flows, but the southeasterly flows remain unexplained by models. It is possible that dust storms originating in Hellas Planitia [e.g., Strausberg *et al.*, 2005], or other flows related to the topography of Hellas, create easterly winds that are strong and persistent enough to dominate dune morphology. However, these dust storms

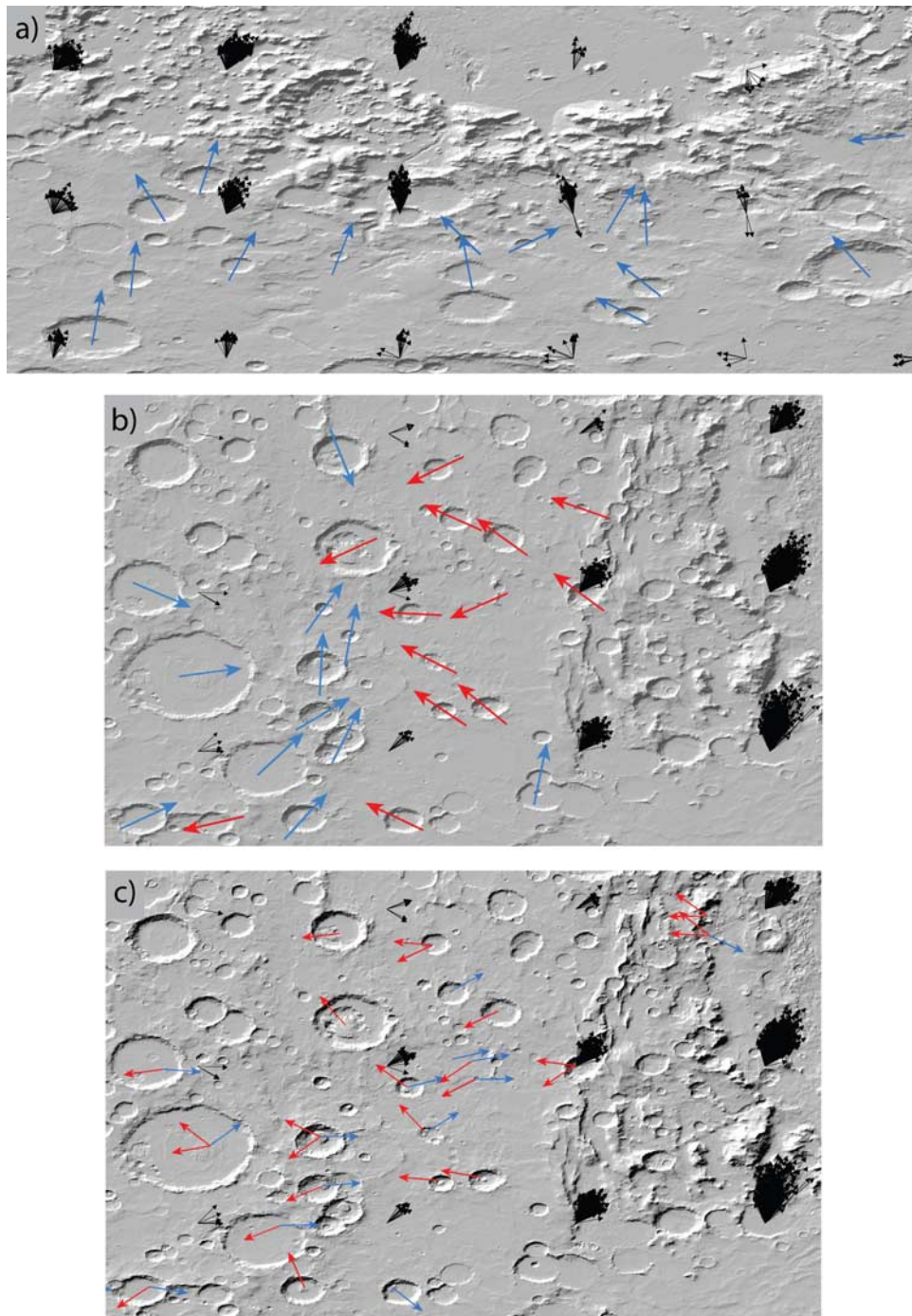


Figure 7. (a) MOLA-derived shaded relief map of the southern rim area of Argyre Planitia. GCM grid wind shear stress vectors (black) correlate well with the dune centroid azimuth vectors (blue), indicating prevailing seasonal winds dominate long-term grain transport in the area, unlike the western rim of Hellas Planitia. (b) MOLA-derived shaded relief map with GCM grid wind shear stress vectors (black) and dune centroid azimuth vectors (red and blue) for the area west of Hellas Planitia. The GCM model predictions suggest grain movement for the area would be approximately from west to east. Red indicates dune centroid azimuth vectors that oppose the GCM, while blue indicates those that agree with the GCM. Within the craters adjacent to Hellas, red vectors predominate, suggesting that long-term grain transport has been opposite GCM predictions. Within the craters more than about 300 km west of Hellas, blue vectors predominate, suggesting long-term grain transport in the same direction as GCM predictions. (c) Same area as Figure 7b with dune slipface vectors. Red indicates slipface vectors that generally oppose the GCM, while blue indicates those that generally agree with the GCM. Both components are more widespread than shown by dune centroid azimuth measurements, suggesting a more multi-dimensional wind regime.

have not been captured by the atmospheric modeling performed to date.

4. Conclusions

[45] From our study of the Martian dunes found between 65°N and 65°S using the MGD³ database several important conclusions can be drawn:

[46] 1. There are several dune forms that do not fit nicely into the standard terrestrial classification system. Additional work needs to be done (and some is in progress) to determine whether a new system of classification is necessary or whether expanding the existing classification system is sufficient.

[47] 2. A large percentage of the dunes identified, classified and measured are transverse in nature and indicate that unidirectional winds are the dominant medium for dune formation on Mars. These results uphold the conclusions based on Mariner and Viking images that unidirectional winds dominate Martian dune morphology [Greeley *et al.*, 1992].

[48] 3. On the basis of our survey of moderate- and large-size dark dune fields, we find that the total areal coverage of such dune fields on Mars may be about 6 times less than on the land (non-ocean) surface area of Earth. Individual dune fields on Mars tend to be smaller in areal extent than terrestrial dune fields, possibly due to (1) the difference in topographic relief, with the cratered surface of Mars providing many small traps, (2) the relative abundance of sand due to the number and magnitude of water-related processes that create sand on Earth, and (3) atmospheric differences that limit sand movement and lengthen timescales of bed-form formation and reconstitution.

[49] 4. The decrease in number, area and volume from high southern latitudes to lower southern latitudes is marked, with 85% of the documented dune fields situated between 30°S and 65°S latitude. This pattern may be related to long-term global wind patterns and the location of source units for the dune material itself.

[50] 5. Slipface orientations of dunes show a fair correlation with the predicted GCM wind azimuths but local topography can exert a greater influence on the slipface orientation than regional prevailing winds.

[51] 6. Dune centroid azimuth appears to be good indicator of long-term grain movement and resultant dune migration directions. Our dune centroid azimuth results indicate that the overall GCM predictions are correct. Because dune centroid azimuth appears to be a good proxy for wind direction, a more detailed look at dune centroid azimuth may help establish sediment transport pathways.

[52] 7. Crater size, with its associated relative physical attribute of smooth versus rough floor topography, appears to be a critical factor in the correlation between dune centroid azimuth and GCM vectors.

[53] 8. Dune centroid azimuth-GCM correlation is greatest in higher southern latitudes because of consistent seasonal wind azimuths, higher shear stress values near the polar cap edge, and many smaller, smooth-floored craters for unhindered dune migration.

[54] 9. A discordance between dune centroid azimuth-GCM correlations exists when compared in the western

Hellas Planitia region and the southern Argyre Planitia region.

[55] 10. MGD³, which includes GCM output, as well as dune type, areal extent, two estimated volumes, slipface azimuth (where possible) and dune centroid azimuth (where applicable) for each of the ~550 dune fields present, has been shown to be a useful tool.

5. Future Work

[56] Later versions of MGD³ will extend geographic coverage to include 65°S to 90°S and 65°N and 90°N latitude, covering the massive polar erg of Olympia Undae and surrounding regions. In addition to the current parameters, it would be valuable to enlarge the database by incorporating other aeolian features, such as TARs, yardangs, wind streaks and dust devil tracks into this digital global version and to distinguish between known active processes and those found to be signatures of previous aeolian regimes. With further study and application, the dune database will provide insight into the Martian aeolian environment and its relationships with global wind patterns, sediment sources, transport pathways, geomorphic features, and erosional and weathering processes, each of which is fundamental to understanding Martian surface history, climate and sediment provenance.

[57] **Acknowledgments.** We appreciate the thoughtful reviews by J. Johnson, J. Hagerty, and K. Tanaka, with a special thanks to J. Skinner for multiple reviews and numerous helpful suggestions. We would also like to thank Ronald Greeley and one anonymous reviewer for suggestions that assisted us in improving the manuscript. We would like to acknowledge funding support from the THEMIS team for this effort. We would like to thank Matt Balme for his assistance, James Torson and Janet Barret for the THEMIS geometry, and the THEMIS targeting team: Laural Cherednik, András Dombovári, Kelly Bender, and Kimberly Murray. Any use of trade or product names in this publication is for descriptive purposes only and does not imply endorsement by the U.S. government.

References

- Bagnold, R. A. (1941), *The Physics of Blown Sand and Desert Dunes*, 265 pp., Methuen, London.
- Balme, M. R., and M. C. Bourke (2005), Preliminary results from a new study of transverse aeolian ridges (TARS) on Mars, *Lunar Planet. Sci.*, XXXVI, Abstract 1892.
- Bass, D. S., and T. Siili (1999), Downslope windstorm effects and raising dust in Hellas Basin (on Mars), *Lunar Planet. Sci.*, XXX, Abstract 1058.
- Bourke, M. C., S. A. Wilson, and J. R. Zimbelman (2003), The variability of transverse aeolian ridges in troughs on Mars, *Lunar Planet. Sci.*, XXXIV, Abstract 2090.
- Bourke, M. C., M. Balme, and J. R. Zimbelman (2004a), A comparative analysis of barchan dunes in the intra-crater dune fields and the North Polar Sand Sea, *Lunar Planet. Sci.*, XXXV, Abstract 1453.
- Bourke, M. C., J. E. Bullard, and O. S. Barnouin-Jha (2004b), Aeolian sediment transport pathways and aerodynamics at troughs on Mars, *J. Geophys. Res.*, 109, E07005, doi:10.1029/2003JE002155.
- Breed, C. S. (1977), Terrestrial analogs of the Hellepontus dunes, Mars, *Icarus*, 30(2), 326–340.
- Breed, C. S., and T. Grow (1979), Morphology and distribution of dunes in sand seas observed by remote sensing, in *A Study of Global Sand Seas*, edited by E. D. McKee, *U.S. Geol. Surv. Prof. Pap.*, 1052, 253–302.
- Breed, C. S., M. J. Grolier, and J. F. McCauley (1979), Morphology and distribution of common “sand” dunes on Mars: Comparison with the Earth, *J. Geophys. Res.*, 84, 8183–8204.
- Byrne, S., and B. C. Murray (2002), North polar stratigraphy and the paleo-erg of Mars, *J. Geophys. Res.*, 107(E6), 5044, doi:10.1029/2001JE001615.
- Christensen, P. R., et al. (2004), The Thermal Emission Imaging System (THEMIS) for the Mars 2001 Odyssey Mission, *Space Sci. Rev.*, 110, 85–130, doi:10.1023/B:SPAC.0000021008.16305.94.
- Cooke, R. U., A. Warren, and A. S. Goudie (1993), *Desert Geomorphology*, 526 pp., Univ. College London Press, London.

- Cutts, J. A., and R. S. U. Smith (1973), Aeolian deposits and dunes on Mars, *J. Geophys. Res.*, **78**, 4139–4154.
- Cwick, G. J., and P. Campos-Marquetti (1983), An analysis of dome-shaped dunes in a portion of the north polar region of Mars, *Prof. Pap.*, **15**, pp. 31–44, Dept. of Geogr. and Geol., Indiana State Univ., Terre Haute.
- De Hon, R. A. (2006), Transitional dune forms on Mars, *Lunar Planet. Sci.*, **XXXVII**, Abstract 1361.
- Edgett, K. S. (2002), Low-albedo surfaces and eolian sediment: Mars Orbiter Camera views of western Arabia Terra craters and wind streaks, *J. Geophys. Res.*, **107**(E6), 5038, doi:10.1029/2001JE001587.
- Edgett, K. S. (2005), The sedimentary rocks of Sinus Meridiani: Five key observations from data acquired by the Mars Global Surveyor and Mars Odyssey orbiters, *Mars*, **1**, 5–58.
- Edgett, K., and P. R. Christensen (1994), Mars aeolian sand: Regional variations among dark-hued crater floor features, *J. Geophys. Res.*, **99**, 1997–2018.
- Edgett, K. S., and M. C. Malin (2000), MGS MOC images of Seif dunes in the north polar region of Mars, Abstract 1070 presented at 31st Annual Lunar and Planetary Science Conference, Lunar and Planet. Inst., Houston, Tex., 13–17 March.
- Fenton, L. K. (2005), Potential sand sources for the dune fields in Noachis Terra, Mars, *J. Geophys. Res.*, **110**, E11004, doi:10.1029/2005JE002436.
- Fenton, L. K., and M. I. Richardson (2001), Martian surface winds: Insensitivity to orbital changes and implications for Aeolian processes, *J. Geophys. Res.*, **106**, 32,885–32,902.
- Fenton, L. K., M. I. Richardson, and A. D. Toigo (2002), Sand transport in Proctor Crater on Mars based on dune morphology and mesoscale modeling, Abstract 1953 presented at 33rd Annual Lunar and Planetary Science Conference, Lunar and Planet. Inst., Houston, Tex., 11–15 March.
- Fenton, L. K., J. L. Bandfield, and A. W. Ward (2003), Aeolian processes in Proctor Crater on Mars: Sedimentary history as analyzed from multiple data sets, *J. Geophys. Res.*, **108**(E12), 5129, doi:10.1029/2002JE002015.
- Fenton, L. K., A. D. Toigo, and M. I. Richardson (2005), Aeolian processes in Proctor Crater on Mars: Mesoscale modeling of dune-forming winds, *J. Geophys. Res.*, **110**, E06005, doi:10.1029/2004JE002309.
- Gaddis, L. R., et al. (1997), An overview of the Integrated Software for Imaging Spectrometers, *Lunar Planet. Sci.*, **XXVIII**, 387–388, Abstract 1226.
- Gorelick, N. S., M. Weiss-Malik, B. Steinberg, and S. Anwar (2003), JMARS: A multimission data fusion application, *Lunar Planet. Sci.*, **XXXIV**, Abstract 2057.
- Greeley, R., R. Leach, B. White, J. Iversen, and J. Pollack (1980), Threshold windspeeds for sand on Mars: Wind tunnel simulations, *Geophys. Res. Lett.*, **7**, 121–124.
- Greeley, R., N. Lancaster, S. Lee, and P. Thomas (1992), Martian aeolian processes, sediments and features, in *Mars*, edited by H. Kieffer et al., pp. 730–766, Univ. of Arizona Press, Tucson.
- Greeley, R., A. Skyeck, and J. B. Pollack (1993), Martian Aeolian features and deposits: Comparison with general circulation model results, *J. Geophys. Res.*, **98**(E2), 3183–3196.
- Greeley, R., M. Kraft, R. Sullivan, G. Wilson, N. Bridges, K. Herkenhoff, R. O. Kuzmin, M. Malin, and W. Ward (1999), Aeolian features and processes at the Mars Pathfinder site, *J. Geophys. Res.*, **104**, 8573–8584.
- Greeley, R. S., et al. (2004), The Athena Science Team; The HRSC Science Team; The Themis Science Team; The Moc Science Team, Coordinated observations of Aeolian features from the Mars Exploration Rovers (MER) and the Mars Express High Resolution Stereo Camera and other orbiters, Abstract 2162 presented at 35th Lunar and Planetary Science Conference, Lunar and Planet. Inst., League City, Tex., 15–19 March.
- Haberle, R. M., M. M. Joshi, J. R. Murphy, J. R. Barnes, J. T. Schofield, G. Wilson, M. Lopez-Valverde, J. L. Hollingsworth, A. F. C. Bridger, and J. Schaeffer (1999), General circulation model simulations of the Mars Pathfinder atmospheric structure investigation/meteorology data, *J. Geophys. Res.*, **104**(E4), 8957–8974.
- Haberle, R. M., J. R. Murphy, and J. Schaeffer (2003), Orbital change experiments with a Mars general circulation model, *Icarus*, **161**, 66–89.
- Hayward, R. K., K. F. Mullins, L. K. Fenton, T. M. Hare, T. N. Titus, M. C. Bourke, T. Colaprete, and P. R. Christensen (2007), Digital Database of Dunes on Mars, *U.S. Geol. Surv. Open File Rep.*, 2007–1158.
- Lancaster, N., and R. Greeley (1990), Sediment volume in the north polar sand seas of Mars, *J. Geophys. Res.*, **95**, 921–927.
- Lee, P., and P. Thomas (1995), Longitudinal dunes on Mars: Relation to current wind regimes, *J. Geophys. Res.*, **100**(E3), 5381–5395.
- Livingstone, I., and A. Warren (1996), *Aeolian Geomorphology: An Introduction*, 211 pp., Addison-Wesley-Longman, Singapore.
- Malin, M. C., G. E. Danielson, A. P. Ingersoll, H. Masursky, J. Veverka, M. A. Ravine, and T. A. Soiland (1992), Mars Observer Camera, *J. Geophys. Res.*, **97**(E5), 7699–7718.
- Malin, M. C., et al. (1998), Early views of the Martian surface from the Mars Orbiter Camera of Mars Global Surveyor, *Science*, **279**, 1681–1685.
- McCauley, J. F., M. H. Carr, J. A. Cutts, W. K. Hartmann, H. Masursky, D. J. Milton, R. P. Sharp, and D. E. Wilhelms (1972), Preliminary Mariner 9 report on the geology of Mars, *Icarus*, **17**, 289–327.
- McKee, E. D. (1979), Introduction to a study of global sand seas, in *A Study of Global Sand Seas*, edited by E. D. McKee, *U.S. Geol. Surv. Prof. Pap.*, **1052**, 3–17.
- Rafkin, S. C. R., R. M. Haberle, and T. I. Michaels (2001), The Mars regional atmospheric modeling system: Model description and selected simulations, *Icarus*, **151**, 228–256.
- Scott, D. H., and K. L. Tanaka (1986), Geologic map of the western equatorial region of Mars, *U.S. Geol. Surv. Misc. Invest. Ser., Map I-1802-A*, 1:15M scale.
- Skinner, J. A., Jr., T. M. Hare, and K. L. Tanaka (2006), Digital renovation of the atlas of Mars 1:15,000,000-scale global geologic series maps, *Lunar Planet. Sci.*, **XXXVII**, Abstract 2331.
- Strausberg, M. J., H. Wang, M. I. Richardson, S. P. Ewald, and A. D. Toigo (2005), Observations of the initiation and evolution of the 2001 Mars global dust storm, *J. Geophys. Res.*, **110**, E02006, doi:10.1029/2004JE002361.
- Tanaka, K. L., J. A. Skinner Jr., T. M. Hare, T. Joyal, and A. Wenker (2003), Resurfacing history of the northern plains of Mars based on geologic mapping of Mars Global Surveyor data, *J. Geophys. Res.*, **108**(E4), 8043, doi:10.1029/2002JE001908.
- Tanaka, K. L., J. A. Skinner Jr., and T. M. Hare (2005), Geologic map of the northern plains of Mars, *U.S. Geol. Surv. Sci. Invest. Ser., Map 2888*.
- Thomas, P. (1984), Martian intra-crater splotches: Occurrence, morphology, and colors, *Icarus*, **57**, 205–227.
- Torson, J. M., and K. J. Becker (1997), ISIS—A software architecture for processing planetary images (abstract), *Lunar Planet. Sci.*, **XXVIII**, 1443–1444.
- Tsoar, H., R. Greeley, and A. R. Peterfreund (1979), Mars: The north polar sand sea and related wind patterns, *J. Geophys. Res.*, **84**, 8167–8180.
- Ward, A. W. (1979), Yardangs on Mars: Evidence of recent wind erosion, *J. Geophys. Res.*, **84**, 8147–8166.
- Ward, A. W., K. B. Doyle, P. J. Helm, M. K. Weisman, and N. E. Witbeck (1985), Global map of eolian features on Mars, *J. Geophys. Res.*, **90**, 2038–2056.
- Wasson, R. J., and R. Hyde (1983), Factors determining desert dune type, *Nature*, **304**, 337–339.
- Wilson (1973), Ergs, *Sediment. Geol.*, **10**, 77–106.

M. C. Bourke, Planetary Science Institute, 1700 East Ft. Lowell Road #106, Tucson, AZ 85719-2395, USA.

P. R. Christensen, Department of Geological Sciences, Arizona State University, Mars Space Flight Facility, Box 876305, Tempe, AZ 85287-6305, USA.

A. Colaprete, NASA Ames Research Center, MS 245-3, Moffett Field, CA 94035-1000, USA.

L. K. Fenton, Carl Sagan Center, NASA Ames Research Center, MS 245-3, Moffett Field, CA 94035-1000, USA.

T. M. Hare, R. K. Hayward, and T. N. Titus, Department of Astrogeology, U.S. Geological Survey, 2255 North Gemini Drive, Flagstaff, AZ 86001, USA.

K. F. Mullins, Science Department, Coconino Community College, 2800 South Lonetree Road, Flagstaff, AZ 86001-2701, USA.